

Quantum Lyapunov exponent in dissipative systems

Pablo D. Bergamasco 

Departamento de Física, CNEA, Libertador 8250, (C1429BNP) Buenos Aires, Argentina

Gabriel G. Carlo and Alejandro M. F. Rivas 

Departamento de Física, CNEA, CONICET, Libertador 8250, (C1429BNP) Buenos Aires, Argentina



(Received 9 November 2022; revised 9 June 2023; accepted 20 July 2023; published 8 August 2023)

The out-of-time order correlator (OTOC) has been widely studied in closed quantum systems. However, there are very few studies for open systems and they are mainly focused on isolating the effects of scrambling from those of decoherence. Adopting a different point of view, we study the interplay between these two processes. This proves crucial in order to explain the OTOC behavior when a phase space contracting dissipation is present, ubiquitous not only in real life quantum devices but in the dynamical systems area. The OTOC decay rate is closely related to the classical Lyapunov exponent—with some differences—and more sensitive in order to distinguish the chaotic from the regular behavior than other measures. On the other hand, it is revealed as a generally simple function of the longest lived eigenvalues of the quantum evolution operator. We find no simple connection with the Ruelle-Pollicott resonances, but by adding Gaussian noise of \hbar_{eff} size to the classical system we recover the OTOC decay rate, which is a consequence of the correspondence principle put forward in *Phys. Rev. Lett.* **108**, 210605 (2012) and *Phys. Rev. E* **99**, 042214 (2019).

DOI: [10.1103/PhysRevE.108.024208](https://doi.org/10.1103/PhysRevE.108.024208)

I. INTRODUCTION

The out-of-time order correlator (OTOC) has been initially introduced in the context of superconductivity, where exponential growth as a function of time has been associated with the behavior of chaotic [1] systems. Pioneering work in black hole theory [2] has led to a resurgence of interest in this measure in various fields such as many-body physics [3–9], high energy theory [10], and quantum chaos [11–14].

The OTOC is conceptually related to quantum information scrambling and complexity [15–20]. For weakly coupled strongly chaotic systems, the OTOC has been found to initially grow in a regime related to intrasubsystem scrambling, while during a second regime it approaches saturation depending on the coupling interaction [20]. On the other hand, OTOC is a good indicator of quantum complexity [21–23]. In this line, an equivalence between the average OTOC over a full basis of operators and the linear entropy has been established through the OTOC-Renyi theorem [24,25]; hence its evaluation allows one to distinguish between regular and chaotic behavior. This equivalence can be obtained in a restricted set of meaningful operators [26], which amounts to defining a preferred OTOC basis.

All these results have been obtained for closed systems, but notably during the past couple of years a strong interest appeared in the OTOC behavior for open systems [27]. Dissipation and information scrambling interplay has been found to manifest in the details of the decay of the four-point out-of-time ordered correlator of local operators [28]. Due to the information loss induced by the environment, the OTOC has been considered not capable of distinguishing between scrambling and decoherence [29]. Instead, mutual information

has been proposed as a better quantifier of these contributions to the information flow [30]. It has only recently been shown that the interplay between information scrambling and decoherence can be used to differentiate between chaotic and regular regimes in dissipative many-body spin chains [31], but only for bipartite OTOC and in an inherently quantum setting. On the other hand, given the importance of OTOCs, multiple measurement protocols have been developed, whose robustness in physically realistic environments remains a subject of investigation [32].

In the context of open quantum systems with a clear classical counterpart, is the OTOC capable of distinguishing between regular or chaotic behavior, as the classical Lyapunov exponent does? In this article we study the OTOC for generic systems of this kind, understood as the quantized versions of typical classical dynamical systems (overwhelmingly studied in the nonlinear dynamics area), by considering the paradigmatic dissipative modified kicked rotator map (DMKRM). For this system and the parameter values explored, we observe that there is no short time Lyapunov exponential growth. However, at longer times ($t > 5$) the OTOC decays exponentially at a rate that closely follows the Lyapunov exponent, regardless of the operators or the initial state. This suggests that the OTOC rate captures the same information about the quantum system's dynamics as the Lyapunov exponent does in classical ones. This decay depends on the forcing and dissipation strengths (K and γ parameters, respectively), which set the degree of scrambling and environmental effects. The interplay between these two processes determines the OTOC decay regime, quantitatively related to the details of the spectral gap of the quantum evolution operator. It is worth mentioning here that the statistical properties of dynamical systems at

the classical level change across local bifurcations, where neither the Lyapunov exponents nor the covariant Lyapunov vectors provide a good criterion for determining the stability of the attractors. Instead, the decay of correlations or mixing, which can be estimated from long times series, are related to the eigenvalues of the generator of the transfer operator semigroup [33].

II. SYSTEM

The OTOC is usually defined as

$$C(t) = \langle [\hat{A}(0), \hat{B}(t)] [\hat{A}(0), \hat{B}(t)]^\dagger \rangle, \quad (1)$$

where \hat{A} and \hat{B} are two operators at different times evolved in the Heisenberg picture. The mean value is taken over a localized initial state $\langle \dots \rangle = \langle \psi_0 | \dots | \psi_0 \rangle$. Nevertheless, the results are the same in the case of considering a thermal initial state [34]. Our classical model consists of a particle moving in one dimension subjected to a periodically kicked asymmetric potential,

$$V(q, t) = k \left[\cos(q) + \frac{a}{2} \cos(2q + \phi) \right] \sum_{m=-\infty}^{\infty} \delta(t - m\tau), \quad (2)$$

where k is the strength of the kick and τ its period. Adding dissipation, we get [35]

$$\bar{n} = \gamma n + k[\sin(q) + \sin(2q + \phi)], \quad \bar{q} = q + \tau \bar{n}, \quad (3)$$

where n (\bar{n}) is the momentum variable conjugate to q (\bar{q}) before (after) the kick and γ ($0 \leq \gamma \leq 1$) is the dissipation parameter. With $\gamma = 1$ we recover the conservative system, while setting $\gamma = 0$ corresponds to maximum environmental strength. Usually, a scaled momentum $p = \tau n$ and the quantity $K = \tau k$ are introduced in order to simplify the expressions. We take $a = 0.5$ and $\phi = \pi/2$ (these parameters are related to spatiotemporal symmetries and at these values provide a rich dynamical landscape suitable for our investigation).

In order to quantize the model, we follow the standard procedure $q \rightarrow \hat{q}$ and $n \rightarrow \hat{n} = -i(d/dq)$ ($\hbar = 1$). Given that $[\hat{q}, \hat{p}] = i\tau$ (where $\hat{p} = \hat{n}$), we define the effective Planck constant by means of identifying $\hbar_{\text{eff}} = \tau$. In the classical limit, $\hbar_{\text{eff}} \rightarrow 0$ and $K = \hbar_{\text{eff}} k$ remains constant. On the other hand, dissipation is treated in the usual way through the Lindblad master equation [36] to describe the evolution of operators in the Heisenberg representation,

$$\dot{\hat{B}} = i[\hat{H}_s, \hat{B}] - \frac{1}{2} \sum_{\nu=1}^2 \{\hat{L}_\nu^\dagger \hat{L}_\nu, \hat{B}\} + \sum_{\nu=1}^2 \hat{L}_\nu^\dagger \hat{B} \hat{L}_\nu \equiv \mathcal{L}(\hat{B}), \quad (4)$$

where $H_s = \hat{n}^2/2 + V(\hat{q}, t)$ is the Hamiltonian of the system, $\{, \}$ is the anticommutator, and \hat{L}_ν are the Lindblad operators defined as [37]

$$\begin{aligned} \hat{L}_1 &= g \sum_n \sqrt{n+1} |n\rangle \langle n+1|, \\ \hat{L}_2 &= g \sum_n \sqrt{n+1} |-n\rangle \langle -n-1|, \end{aligned} \quad (5)$$

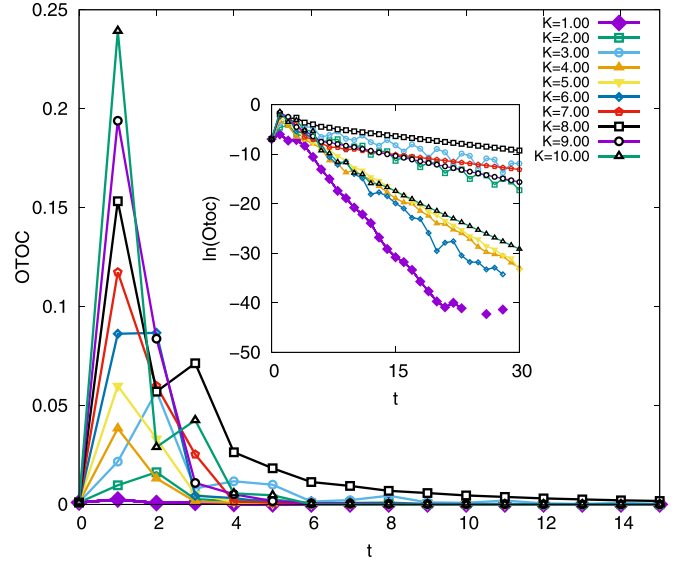


FIG. 1. OTOC as a function of time t for different values of K represented by lines with symbols (see legend). The inset shows the same evolution in log scale. In this case $\hbar_{\text{eff}} = 0.031$, $\gamma = 0.200$, and the dimension of Hilbert space is $N = 1024$.

where $|n\rangle$ are the momentum states with $n = 0, 1, \dots$ and $g = \sqrt{-\ln \gamma}$ [38,39].

III. RESULTS

In the following we compare the OTOC behavior in several areas of the parameter space (corresponding to different dynamical regimes), both with the inverse participation ratio (IPR) (another widely used quantum complexity measure) and the (classical) Lyapunov exponent which allows distinguishing between regular and chaotic behavior efficiently. We use the operators $\hat{A} = e^{i\hat{Q}}$ and $\hat{B} = \hat{P}$ in Eq. (1), where \hat{Q} is the position operator and \hat{P} is the momentum operator. The evolution of \hat{B} is given by Eq. (4) integrated between t and $t + 1$, i.e., we are looking at the state of the system between successive potential kicks. As an initial condition, we have used a coherent state centered at $\langle p_0 \rangle = 0$ and $\langle q_0 \rangle = \pi$. In the classical case, we numerically evaluate Eq. (3). Our results have been shown to be robust against a change in the operators \hat{A} , \hat{B} considered for the calculations (see the Appendix). In Fig. 1 we observe the OTOC evolution up to a time $t = 15$ for different values of K . In all cases we have taken a value of $\hbar_{\text{eff}} = 0.031$ and $\gamma = 0.20$. The results for other values of γ and \hbar_{eff} are presented in the Appendix. The OTOC initially grows very fast and then decays exponentially (log scale in the inset). In chaotic closed systems the OTOC growth has been found to be exponential with a rate given by the Lyapunov exponent of its classical counterpart. Interestingly, in our case we do not find that kind of growth, though given its extremely fast nature we cannot be conclusive about a general behavior. In Fig. 2 we compare the maximum Lyapunov exponent $\langle l_{\text{max}} \rangle_M$, averaged over M initial conditions, and (q_0, p_0) distributed with uniform probability in the region $[0, 2\pi] \times [-\pi, \pi]$.

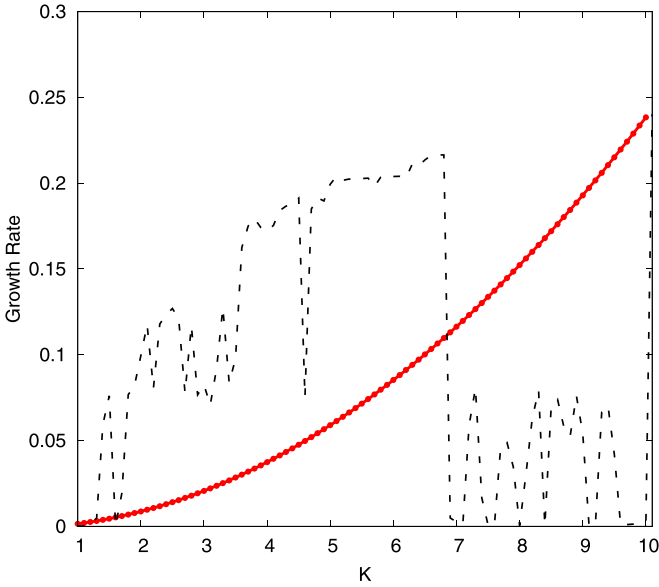


FIG. 2. (Red) dark gray solid line with circles shows the growth rate of the OTOC of Fig. 1 between $t = 0$ and $t = 1$, as a function of K . The black dashed line displays the average maximum Lyapunov exponent as a function of the same parameter of the classical system (in all cases $\gamma = 0.20$).

We have calculated the OTOC decay rate by fitting $\ln(\text{OTOC})$ for values of K from 1 to 10 and compared it with the maximum average Lyapunov exponent $l_{\max} = \langle I_{\max}^{(i)} \rangle_M$ and

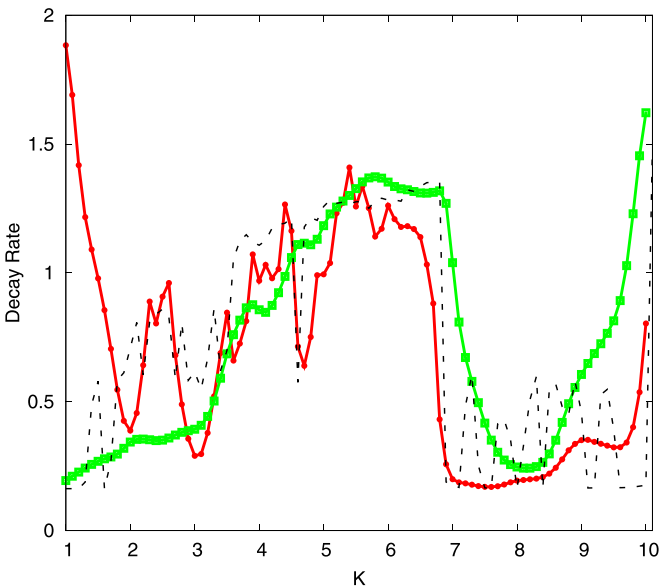


FIG. 3. (Red) dark gray solid line with circles shows the decay rate of the OTOC of Fig. 1 between $t = 5$ and $t = 100$, as a function of K . The (green) light gray solid line with squares corresponds to the quantum IPR values and the black dashed line to the average maximum Lyapunov exponent of the classical system (in all cases $\gamma = 0.200$).

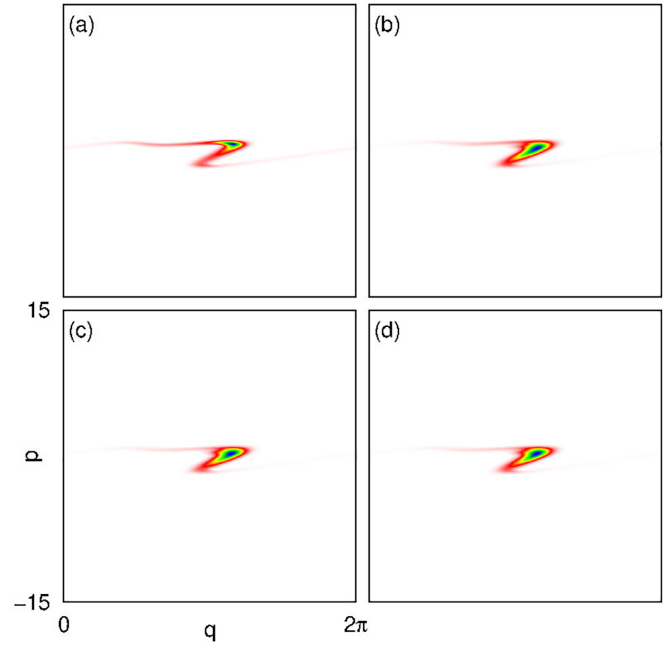


FIG. 4. Phase space representation of the evolved initial state for times (a) $t = 1$, (b) $t = 3$, (c) $t = 8$, and (d) $t = 20$. Lower to higher values of the distributions go from white to (rainbow colors) darker grays. In this case $K = 1.10$, $\hbar_{\text{eff}} = 0.031$, $\gamma = 0.200$, and the dimension of Hilbert space is $N = 1024$.

the IPR defined as

$$\text{IPR} = \frac{(\sum \rho_{ii}^2)^{-1}}{N},$$

with ρ_{ii} being the diagonal elements of the density matrix of the steady state in the momentum basis. The results are shown in Fig. 3 where the Lyapunov exponent and IPR were rescaled according to $\tilde{l}_{\max} = 0.55 l_{\max} + 0.605$ and $\tilde{\text{IPR}} = 3.5 \text{IPR}$. The horizontal line at 0.605 corresponds to zero value for the Lyapunov exponent, i.e., the border between the chaotic and regular regimes. First, we can observe that for $K > 2$ the OTOC decays at a lower rate in regular regions, which in turn correspond to a Lyapunov exponent of less than 0.605. However, for $K < 2$ we see that the behavior of the OTOC disagrees with that of the Lyapunov exponent. This can be explained given that the strength of the kick is not enough for the system to explore a significant portion of the phase space and therefore the OTOC cannot account for enough scrambling, decaying before that can happen due to dissipation. This is clearly seen by looking at the evolution of the Husimi functions for $K = 1.10$ displayed in Fig. 4. At larger values of K , a much greater region of phase space is explored and the OTOC is able to capture the interplay between scrambling and decoherence. In the region $2 < K < 7$ the system is mainly chaotic, with specific K values for which regularity is recovered. This can be learned from the Lyapunov exponent and the bifurcation diagram of Fig. 5. The larger regular regions in this portion of the parameter space are detected by the OTOC as can be seen by the decay rate abrupt changes. On the other hand, for $K > 7$, the OTOC detects very well the beginning and ending of the largest regular

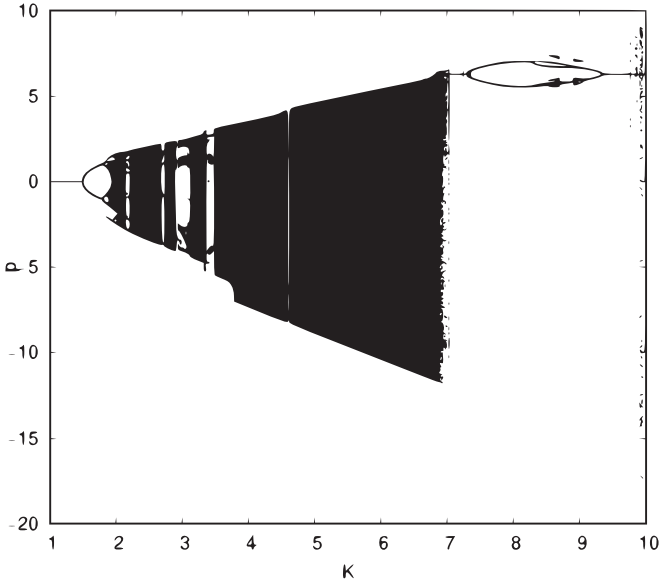


FIG. 5. Bifurcation diagram for the classical system given by Eq. (3) for $\gamma = 0.200$.

region, in agreement with what is shown by the Lyapunov exponent and the classical bifurcation diagram. In contrast, the IPR fails to sharply account for both limits, reflecting an effectively smaller regular window. This is because the IPR relies only on the equilibrium state distribution, which suffers from *parametric tunneling* [40]. The consequences for our understanding of this phenomenon arising from this dis-

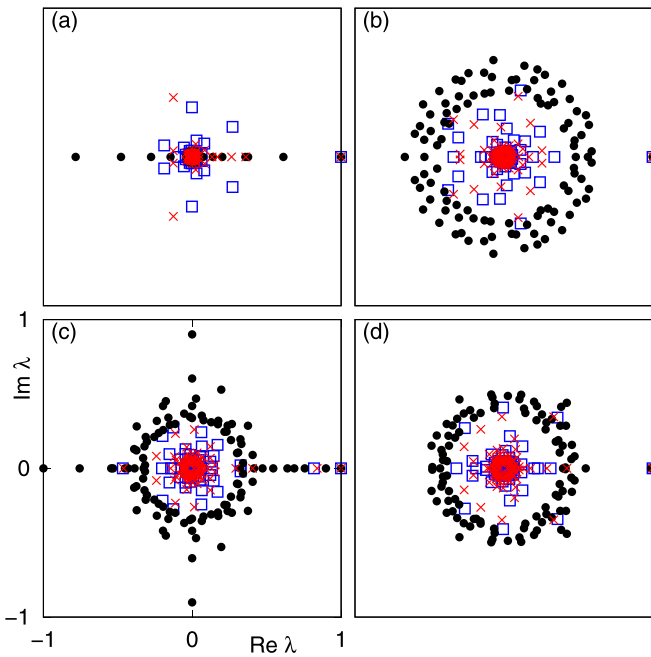


FIG. 6. 100 largest eigenvalues of the quantum superoperator $\Lambda = \exp(\mathcal{L})$ and of the Perron-Frobenius operator with and without Gaussian noise, for (a) $K = 1.10$, (b) $K = 5.40$, (c) $K = 8.20$, and (d) $K = 10.00$. (Blue) gray squares correspond to the quantum model and red crosses and black dots to the classical one with and without Gaussian noise, respectively. In this case, $\hbar_{\text{eff}}^{(\text{PF})} = \hbar_{\text{eff}} = 0.150$, $\gamma = 0.200$, and the dimension of Hilbert space is $N = 512$.

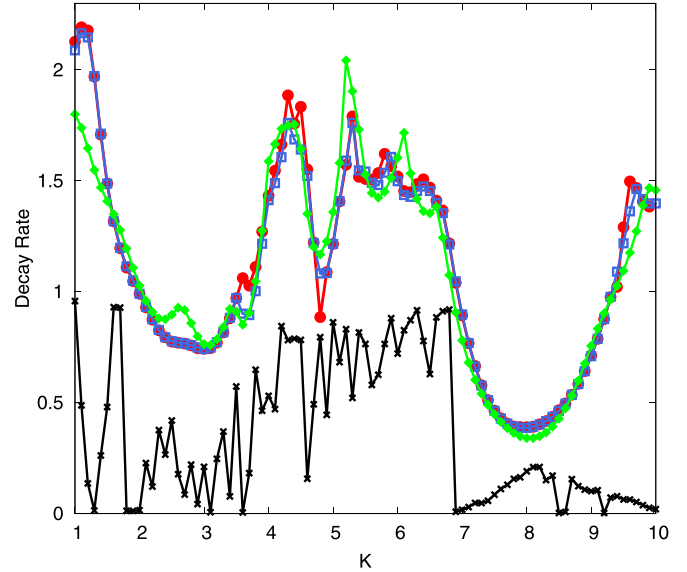


FIG. 7. (Red) dark gray solid line with circles shows the decay rate of the OTOC between $t = 5$ and $t = 100$, as a function of K . The (blue) gray solid line with empty squares represents $-2 \ln(|\lambda_1|)$ for the eigenvalue λ_1 of the quantum evolution operator and the (green) light gray solid line with diamonds and black solid line with crosses correspond to the same quantity but for the classical system with and without Gaussian noise, respectively. In all cases $\hbar_{\text{eff}}^{(\text{PF})} = \hbar_{\text{eff}} = 0.150$, $\gamma = 0.200$, and $N = 512$.

crepancy will be explored in subsequent work. We underline here that the OTOC behavior remains essentially unchanged when considering a thermal instead of a coherent state for the calculations (see the Appendix). In the classical system, the Perron-Frobenius operator determines the evolution of Liouville distributions, while in its quantum counterpart this is accomplished by the Lindblad operator \mathcal{L} acting on the density matrix as $\rho_{t+1} = \exp(\mathcal{L})\rho_t = \Lambda\rho_t$. Both have an eigenvalue $\lambda_0 = 1$, whose eigenvector is the attractor to which the initial conditions decay when $t \rightarrow \infty$. The other leading eigenvalues of modulus less than one prescribe the decays. At the classical level, we use Ulam's method to obtain an approximation of the Perron-Frobenius operator from the discretization of the system into cells of size $\hbar_{\text{eff}}^{(\text{PF})}$. Figure 6 shows the 100 largest quantum and classical eigenvalues for different values of K ; clear differences between the spectra can be seen (we have used $\hbar_{\text{eff}}^{(\text{PF})} = \hbar_{\text{eff}} = 0.150$ to reduce the basis size in which the Perron-Frobenius operator is discretized since this is a computationally demanding task). The spectral gap is given by λ_1 —the decaying eigenvalue with the largest modulus. Figure 7 shows the OTOC decay rate together with $-2 \ln(|\lambda_1|)$ from both the quantum and classical spectra as a function of K . The agreement between the OTOC and the quantum spectral decay is generally very good, even for low K . There are values at which the differences are noticeable though, for example, at $K \approx 3.5$. This is due to the fact that in this parameter region chaotic and regular behavior coexist as observed in the bifurcation diagram of Fig. 5. On the other hand, the decay rate associated to the classical spectrum behaves very differently, implying that the OTOC is not directly predicted by the Ruelle-Pollicott resonances in a simple way.

In [37] these discrepancies proved to be drastically reduced by adding Gaussian noise ξ (with $\langle \xi \rangle = 0$ and $\langle \xi \rangle^2 = \hbar_{\text{eff}}$) only to the classical system. If we do this, the disagreement between the classical and the OTOC decay rates disappear and the quantum to classical correspondence is recovered.

IV. CONCLUSIONS

To summarize our findings, we have observed that the out-of-time-ordered correlator (OTOC) in the quantum dissipative modified kicked rotator model (DMKRM) exhibits rapid growth at short times, followed by exponential decay at a rate that closely follows the rescaled Lyapunov exponent of the classical DMKRM. While we do not suggest that the decay rate can be quantitatively derived from the Lyapunov exponent, we do find that both metrics provide similar insights into the distinct dynamical regimes of the system. As such, we refer to it as the quantum Lyapunov. This decay depends on the dissipation and forcing strengths γ and K , which determine the chaotic or regular nature of the dynamics. Moreover, the OTOC revealed itself as much more sensitive to the dynamical regime type when compared with other complexity measures based on the eigenstates' distributions, like the very frequently used IPR. However, when the distributions are not able to explore a meaningful portion of phase space the scrambling power of the system is not sufficiently captured by the OTOC, and consequently it becomes a poor complexity detector as happens for $K < 2$ in our model. All this points towards the fact that capturing the interplay between scrambling and dissipation is of the essence at the time to characterize the complexity of quantum dissipative systems. In the vast majority of the dynamical scenarios we have looked into, studying the OTOC showed as a very suitable way to do it. On the other hand, the largest decaying eigenvalue λ_1 determines in almost the entire range of K the decay rate of the OTOC, except for a few small regions to be analyzed in more detail in future work. We recall that changes in the classical eigenvalue spectrum indicate the loss or gain of stability of the attractor [33]; therefore, the OTOC could be a good way to extend this result to the quantum realm. Finally, by adding \hbar_{eff} -sized Gaussian noise only to the classical system, we recover the OTOC decay rate as being a nice example of the quantum to classical correspondence principle of quantum dissipative systems [37,41]. Though we have extensively shown the robustness of our results in a paradigmatic system, we consider that exploring other scenarios is an interesting avenue for the future. Deeper theoretical open questions about the OTOC behavior in dissipative systems, like the link between its approximate Lyapunov decay and the spectral features, will surely inspire more work in the field [42].

ACKNOWLEDGMENT

Financial support from CONICET is gratefully acknowledged.

APPENDIX: ADDITIONAL RESULTS

In this Appendix, we provide additional results to support our findings. Specifically, we show that the decay rate

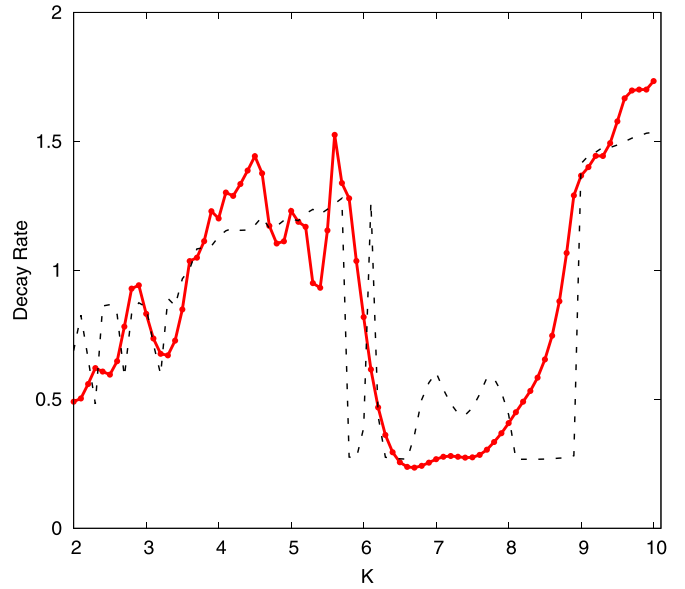


FIG. 8. (Red) dark gray solid line with circles shows the decay rate of the OTOC between $t = 5$ and $t = 100$, as a function of K for a coherent initial state at $(q, p) = (\pi, 0)$. The black dashed line displays the average maximum Lyapunov exponent as a function of the same parameter of the classical system. In all cases $\hbar_{\text{eff}} = 0.068$, $\gamma = 0.290$, and $N = 1024$.

of the out-of-time-ordered correlator (OTOC) is robustly related to both the spectral gap and the Lyapunov exponent of its classical counterpart. We also show that this decay rate is essentially independent of the initial state

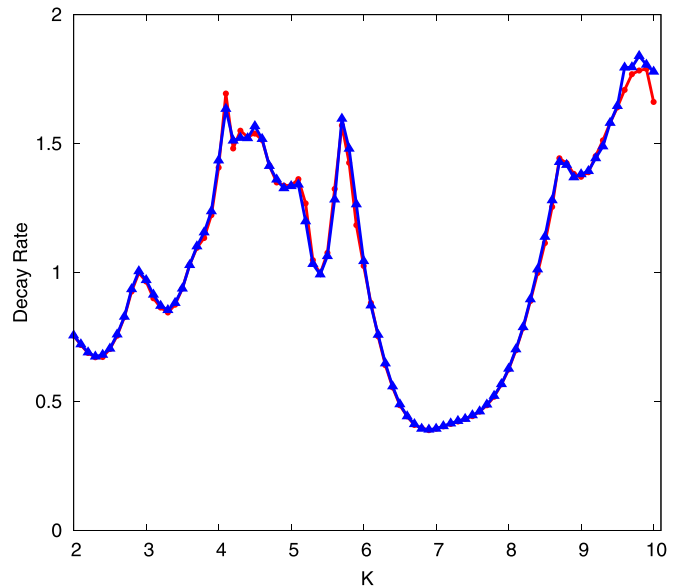


FIG. 9. (Red) dark gray solid line with circles shows the decay rate of the OTOC between $t = 5$ and $t = 100$, as a function of K for a coherent initial state at $(q, p) = (\pi, 0)$. The (blue) gray solid line with triangles corresponds to the initial coherent state placed at $(q, p) = (0, 2\pi)$. In these cases we have taken $\hbar_{\text{eff}} = 0.137$, $\gamma = 0.290$, and $N = 1024$.

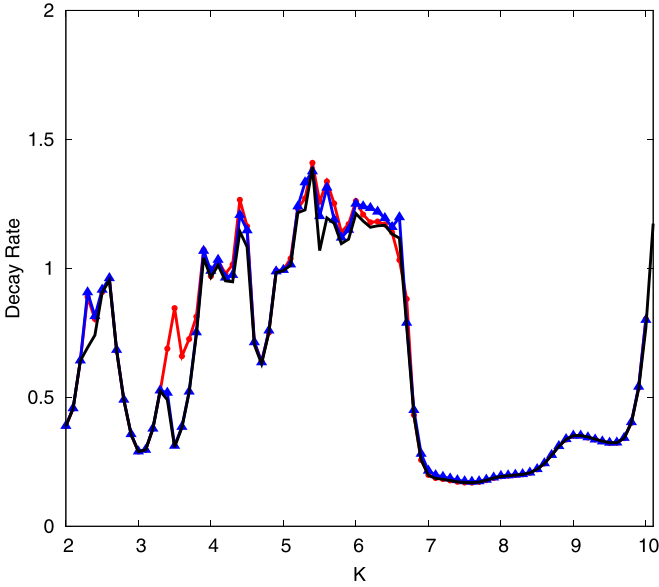


FIG. 10. (Red) dark gray solid line with circles shows the decay rate of the OTOC between $t = 5$ and $t = 100$, as a function of K for a coherent initial state at $(q, p) = (\pi, 0)$. The (blue) gray solid line with triangles corresponds to the thermal initial state. The black solid line represents $-2 \ln(|\lambda_1|)$. In all cases $\hbar_{\text{eff}} = 0.031$, $\gamma = 0.200$, and $N = 1024$.

of the system and the choice of operators \hat{A} and \hat{B} in Eq. (1).

1. Different dissipation parameter γ

Previously we considered $\gamma = 0.20$ and $\hbar_{\text{eff}} = 0.031$ —values at which the system displays a rich diversity of dynamical behavior as a function of K and the computational cost is reasonable. This is also the case for $\gamma = 0.29$ and $\hbar_{\text{eff}} = 0.068$, where, as shown in Fig. 8, a similar correlation between the OTOC decay and the Lyapunov exponent can be verified. As can be observed, a large value of \hbar_{eff} increases the differences between classical and quantum measures. However, the correspondence is restored by introducing Gaussian noise of size \hbar_{eff} into the classical system, as shown in Fig. 7.

2. Independence on the initial state

Results do not depend on the location of the coherent initial state. In fact, we have considered a different position than the one studied in the main text, i.e., $(q, p) = (0, 2\pi)$. The comparison can be made by inspecting Fig. 9 ($\gamma = 0.290$ and

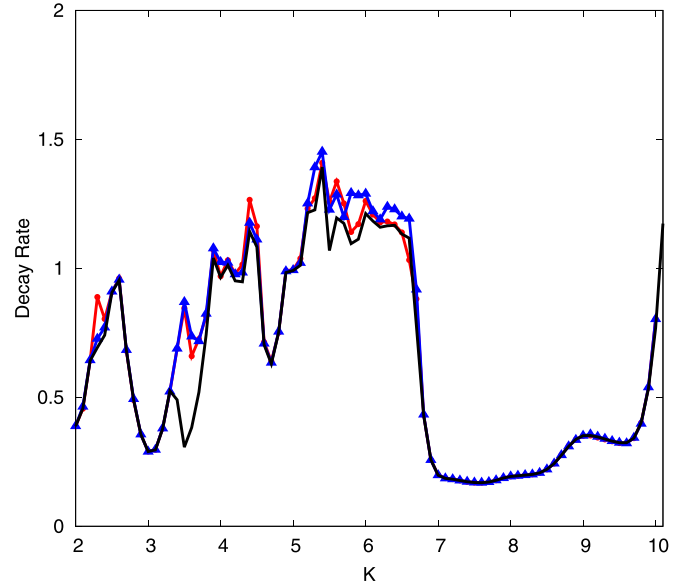


FIG. 11. (Red) dark gray solid line with circles shows the decay rate of the OTOC between $t = 5$ and $t = 100$, as a function of K , with $\hat{A} = e^{i\hat{Q}}$ and $\hat{B} = \hat{P}$. The (blue) gray solid line with triangles corresponds to $\hat{A} = e^{i\hat{Q}}$ and $\hat{B} = e^{i\hat{Q}}\hat{P}$. The black solid line represents $-2 \ln(|\lambda_1|)$. In both cases, we considered an initial coherent state placed at $(q, p) = (0, 2\pi)$ and $\hbar_{\text{eff}} = 0.031$, $\gamma = 0.200$, and $N = 1024$.

$\hbar_{\text{eff}} = 0.137$). Moreover, if we take an initial thermal state $\rho = \mathbb{I}/N$, the decay of the OTOC is essentially the same; this can be checked by means of Fig. 10. While underlining this overwhelming coincidence, we would like to note that there are some very small differences at around $K = 3.50$ between the coherent and thermal state scenarios, with this latter perfectly matching the decay rate values extracted from the spectral gap. We conjecture that these minor differences are due to the fact that in this parameter region the attractor is approached through a simple limit cycle of period 3, which translates into a more complex spectral behavior. Further investigation along this line will be carried out elsewhere.

3. Independence on the choice of operators

Finally, in Fig. 11, results are shown for two sets of operators \hat{A} and \hat{B} in Eq. (1). In the first case, we choose $\hat{A} = e^{i\hat{Q}}$ and $\hat{B} = \hat{P}$ and, in the second case, we change \hat{B} to $e^{i\hat{Q}}\hat{P}$. Again, we observe that the OTOC decay rate is the same for both sets of operators, allowing us to obtain equivalent information about the dynamics of the system.

- [1] A. I. Larkin and Yu. N. Ovchinnikov, *Sov. Phys. JETP* **28**, 1200 (1969).
- [2] J. M. Maldacena, S. H. Shenker, and D. Stanford, *J. High Energy Phys.* **08** (2016) 106.
- [3] S. H. Shenker and D. J. Stanford, *J. High Energy Phys.* **03** (2014) 067.
- [4] I. L. Aleiner, L. Faoro, and L. B. Ioffe, *Ann. Phys. (Amsterdam)* **375**, 378 (2016).

- [5] Y. Huang, Y.-L. Zhang, and X. Chen, *Ann. Phys. (Berlin)* **529**, 1600318 (2017).
- [6] F. Borgonovi and F. M. Izrailev, *Phys. Rev. E* **99**, 012115 (2019).
- [7] K. Slagle, Z. Bi, Y. Z. You, and C. Xu, *Phys. Rev. B* **95**, 165136 (2017).
- [8] X. Chen, T. Zhou, D. A. Huse, and E. Fradkin, *Ann. Phys. (Berlin)* **529**, 1600332 (2017).

- [9] E. M. Fortes, I. García-Mata, R. A. Jalabert, and D. A. Wisniacki, *EPL* **130**, 60001 (2020).
- [10] T. Akutagawa, K. Hashimoto, T. Sasaki, and R. Watanabe, *J. High Energy Phys.* **08** (2020) 013.
- [11] T. Notenson, I. García-Mata, A. J. Roncaglia, and D. A. Wisniacki, *Phys. Rev. E* **107**, 064207 (2023).
- [12] A. Lakshminarayan, *Phys. Rev. E* **99**, 012201 (2019).
- [13] J. Wang, G. Benenti, G. Casati, and W. G. Wang, *Phys. Rev. E* **103**, L030201 (2021).
- [14] R. A. Jalabert, I. García-Mata, and D. A. Wisniacki, *Phys. Rev. E* **98**, 062218 (2018).
- [15] S. Pappalardi, A. Russomanno, B. Žunkovič, F. Iemini, A. Silva, and R. Fazio, *Phys. Rev. B* **98**, 134303 (2018).
- [16] M. Campisi and J. Goold, *Phys. Rev. E* **95**, 062127 (2017).
- [17] B. Swingle, *Nat. Phys.* **14**, 988 (2018).
- [18] V. Balachandran, G. Benenti, G. Casati, and D. Poletti, *Phys. Rev. B* **104**, 104306 (2021).
- [19] J. Wang, G. Benenti, G. Casati, and W. G. Wang, *Phys. Rev. Res.* **2**, 043178 (2020).
- [20] R. Prakash and A. Lakshminarayan, *Phys. Rev. B* **101**, 121108(R) (2020).
- [21] P. D. Bergamasco, G. G. Carlo, and A. M. F. Rivas, *Phys. Rev. E* **96**, 062144 (2017).
- [22] G. Benenti, G. G. Carlo, and T. Prosen, *Phys. Rev. E* **85**, 051129 (2012).
- [23] P. D. Bergamasco, G. G. Carlo, and A. M. F. Rivas, *Phys. Rev. Res.* **1**, 033044 (2019).
- [24] P. Hosur, X. L. Qi, D. A. Roberts, and B. Yoshida, *J. High Energy Phys.* **02** (2016) 004.
- [25] R. Fan, P. Zhang, H. Shen, and H. Zhai, *Sci. Bull.* **62**, 707 (2017).
- [26] P. D. Bergamasco, G. G. Carlo, and A. M. F. Rivas, *Phys. Rev. E* **102**, 052133 (2020).
- [27] J. R. González Alonso, N. Yunger Halpern, and J. Dressel, *Phys. Rev. Lett.* **122**, 040404 (2019).
- [28] Y.-L. Zhang, Y. Huang, and X. Chen, *Phys. Rev. B* **99**, 014303 (2019).
- [29] A. Touil and S. Deffner, *Quantum Sci. Technol.* **5**, 035005 (2020).
- [30] A. Touil and S. Deffner, *PRX Quantum* **2**, 010306 (2021).
- [31] P. Zanardi and N. Anand, *Phys. Rev. A* **103**, 062214 (2021).
- [32] B. Swingle and N. Yunger Halpern, *Phys. Rev. A* **97**, 062113 (2018).
- [33] A. Tantet, V. Lucarini, and H. A. Dijkstra, *J. Stat. Phys.* **170**, 584 (2018).
- [34] I. García-Mata, M. Saraceno, R. A. Jalabert, A. J. Roncaglia, and D. A. Wisniacki, *Phys. Rev. Lett.* **121**, 210601 (2018).
- [35] G. G. Carlo, G. Benenti, G. Casati, and D. L. Shepelyansky, *Phys. Rev. Lett.* **94**, 164101 (2005).
- [36] G. Lindblad, *Commun. Math. Phys.* **48**, 119 (1976).
- [37] G. G. Carlo, L. Ermann, and A. M. F. Rivas, *Phys. Rev. E* **99**, 042214 (2019).
- [38] R. Graham, *Z. Phys. B* **59**, 75 (1985).
- [39] T. Dittrich and R. Graham, *Europhys. Lett.* **7**, 287 (1988); *Ann. Phys. (N.Y.)* **200**, 363 (1989).
- [40] L. Ermann and G. G. Carlo, *Phys. Rev. E* **91**, 010903(R) (2015).
- [41] G. G. Carlo, *Phys. Rev. Lett.* **108**, 210605 (2012).
- [42] P. D. Bergamasco, G. G. Carlo, and A. M. F. Rivas (unpublished).